Progress In Electromagnetics Research B, Vol. 94, 19–36, 2021

Inversion of Electrical and Geometrical Parameters of a Stratified Medium from Data Derived from the Small Perturbation Method and the Small Slope Approximation

Nada Djedouani[1], Saddek Afifi[1], and Richard Dusséaux[2, *]

Abstract—The goal of the present paper is on retrieving the electrical and geometrical parameters of a stratified medium with two rough interfaces. The inversion problem is formulated as a cost function optimization problem, and it is solved using the simulated annealing algorithm. The cost function consists in the integrated squared deviation between the co-polarized incoherent intensities obtained from the Small Slope Approximation and those obtained from the Small Perturbation Method. The inversion scheme is applied to the electrical and geometrical parameters involved into the analytical expressions of the incoherent intensities given by the SPM. We study the influence of the shape of the autocorrelation function and the isotropy factor upon the estimation of parameters. We test the sensitivity of the inversion scheme to noisy synthetic data. The study is applied to snow-covered soils in L-band. For the configurations under study, we show that the inverse method is efficient for eight-parameter or ten-parameter predicting problems.

1. INTRODUCTION

Scattering of electromagnetic waves from layered rough surface structures has aroused the interest of physicists and engineers for many years because of its wide range of applications in remote sensing, geophysics, or optics. Monostatic and bi-static radars allow the study of these structures by measuring backscattered and scattered signals. For a layered structure with rough boundaries, the scattered signal depends on the roughness of each interface and on the thickness and the complex relative permittivity of each layer. It varies depending on the frequency and polarization of the incident wave and on the observation and incidence angles.

Electromagnetic modeling is a valuable tool for radar data inversion to intend to characterize the geometrical and electrical properties of layered structures. The analytical models are based on physical approximations which reduce the applicability domain [1–3]. Within their domains of applicability, these models allow a fast analysis of the multilayered structures by means of analytical formulae. The second class of electromagnetic models relies on numerical methods for solving Maxwell's equations and boundary conditions [4–9]. These models are called exact if no physical approximation is made. These models require Monte-Carlo simulations and do not provide an analytical solution of the scattering problem and require high computational times. This is a major drawback for the inversion of radar data.

The estimation of the electrical and geometrical parameters can be obtained from the minimization of a cost function built from electromagnetic model and experimental data [10–12], and a conventional minimization approach is applied to find the smallest possible value of the cost function. The main

Received 13 July 2021, Accepted 26 September 2021, Scheduled 10 October 2021
* Corresponding author: Richard Dusséaux (richard.dusseaux@latmos.ipsl.fr).
[1] Laboratoire d'Etude et de Recherche en Instrumentation et en Communication d'Annaba (LERICA), Badji Mokhtar-Annaba, University, Annaba 23000, Algeria. [2] Université de Versailles Saint-Quentin-en-Yvelines — Paris-Saclay, LATMOS, 11 Boulevard d'Alembert, Guyancourt 78280, France.

disadvantage of an optimization approach is that a rather large number of direct-scattering problems must be resolved to obtain a satisfactory estimation. As a result, the optimization approach is relatively time-consuming, and it is therefore preferable to use an analytical model in the cost function. In [13], the parameters of a stack of two random rough interfaces are estimated from synthetic data that consist of the backscattered incoherent intensities for multiple polarizations, frequencies, and incidence and observation zenith angles. The authors use the small perturbation method to solve the direct problem [14–21]. The inversion problem is expressed as a least square problem, and it is solved using a simulated annealing algorithm [22–26]. Both rough interfaces are assumed uncorrelated and the autocorrelation functions, isotropic. Complex dielectric constants of the central and lower layers, central layer thickness, root-mean-square height, and correlation length of each rough interface are the unknowns in this inverse scattering problem. The sensitivity of the inversion scheme to noise on the synthetic data is studied, and the efficiency of the inversion algorithm is shown.

The goal of the present paper is on retrieving the electrical and geometrical parameters of a stratified medium with two rough interfaces. We use the inversion scheme defined in [13] and study the sensitivity of the optimization approach to data noise. We consider mono-frequency bi-static radar configurations. The synthetic data are the co-polarized incoherent intensities obtained from the first-order Small Slope Approximation (SSA) [27–32]. The SSA has a wider validity domain than that of the Small Perturbation Method (SPM) and bridges the gap between the SPM and the Kirchhoff Approximation that is applicable to large radius of curvature compared to the wavelength [33]. The cost function consists in the integrated squared deviation between the incoherent intensities obtained from the SSA and those obtained from the SPM. The inversion scheme is applied to the electrical and geometrical parameters involved into the analytical expressions of the co-polarized incoherent intensities given by the SPM. We study the influence of the shape of the autocorrelation function upon the estimation of parameters. We consider bi-exponential and Gaussian functions. We also consider anisotropic correlation functions and define configurations in order to obtain a satisfactory estimation of all correlations lengths. The study is applied to snow-covered soils in L-band [34–36].

This paper is organized as follows. In Section 2, we present the statistical properties of the three dimensional layered structure under consideration and define the interface spectra for Gaussian and bi-exponential correlation functions, with or without anisotropy. In Section 3, we give expressions for the co-polarized incoherent intensities within the framework of the SPM and SSA. Section 4 introduces the inverse problem and cost function. Section 5 is devoted to the study of inversion scheme for snow-covered soils, and the resistance of the inversion algorithm to noise of synthetic data is analyzed.

2. GEOMETRY OF THE PROBLEM

As shown in Fig. 1, we consider a geometric problem where two rough interfaces separate three regions.

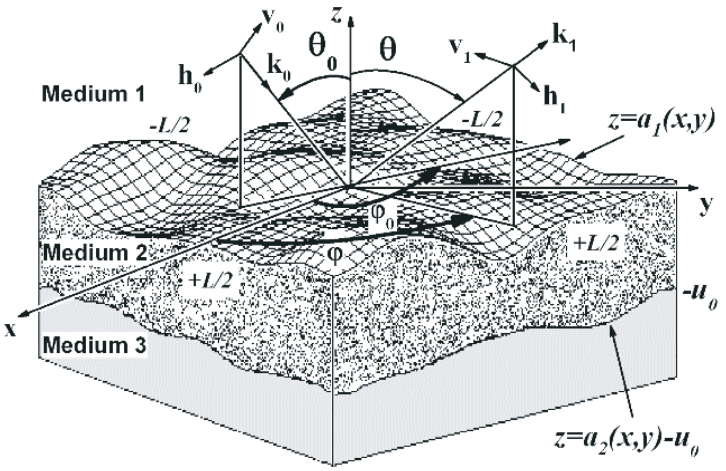

Figure 1. Structure with two nonparallel interfaces.

Region 1 is assumed to be air (assimilated to vacuum). The bottom region is a half-space. The average thickness of region 2 is denoted by u_0. The two boundaries are located at the heights $z = a_1(x, y)$ and $z = a_2(x, y) - u_0$. The non-parallel interfaces are randomly deformed over an area $L \times L$. They are realizations of second order stationary, uncorrelated, and centered Gaussian stochastic processes. Each process is characterized by a statistical autocorrelation function $R_{ii}(x, y)$ given by Eq. (1).

$$R_{ii}(x,y) = \sigma_{a_i}^2 \exp\left[-\left(\sqrt{\frac{x^2}{l_{xi}^2} + \frac{y^2}{l_{yi}^2}}\right)^{2r_e}\right] \tag{1}$$

The quantity r_e designates the roughness exponent. The autocorrelation function is a Gaussian function when $r_e = 1$ and a bi-exponential one when $r_e = 0.5$. The quantity σ_{a_i} is the standard deviation of the i-th interface heights. There are two correlation lengths, l_{xi} and l_{yi}. The i-th interface is isotropic if $l_{xi} = l_{yi}$ and anisotropic if $l_{xi} \neq l_{yi}$. The roughness spectrum $\hat{R}_{ii}(\alpha, \beta)$ is expressed in the following form:

$$\hat{R}_{ii}(\alpha,\beta) = \sigma_{a_i}^2 l_{xi} l_{yi} \pi \exp\left(-\alpha^2 \frac{l_{xi}^2}{4} - \beta^2 \frac{l_{yi}^2}{4}\right) \quad \text{when} \quad r_e = 1 \tag{2}$$

$$\hat{R}_{ii}(\alpha,\beta) = \frac{2\pi\sigma_{a_i}^2 l_{xi} l_{yi}}{\left(1 + \alpha^2 l_{xi}^2 + \beta^2 l_{yi}^2\right)^{3/2}} \quad \text{when} \quad r_e = 0.5 \tag{3}$$

Throughout the paper, a function with an exponent "$\wedge$" denotes the Fourier transform of the function. The quantities α and β are the wave numbers resulting from the 2D Fourier transform of the autocorrelation function.

3. DIRECT MODELS FOR THE INCOHERENT INTENSITY

A monochromatic h- or v-polarized plane wave of wavelength λ impinges on the structure. The incident wave vector $k_0(\alpha_0, \beta_0, -\gamma_0)$ is defined by the zenith angle θ_0 and the azimuth angle φ_0 (Fig. 1) with $\alpha_0 = k_1 \sin\theta_0 \cos\varphi_0$, $\beta_0 = k_1 \sin\theta_0 \sin\varphi_0$ and $\gamma_0 = k_1 \cos\theta_0$. Each region (m) is an isotropic, homogenous medium characterized by its complex relative permittivity ε_{rm} and the wave number $k_m = \sqrt{\varepsilon_{r_m}} k_0$ where k_0 is the vacuum wave number ($k_1 = k_0$).

For an observation direction defined by angles θ and φ (see Fig. 1), the SPM gives the first-order amplitudes of the co- and cross-polarized contributions of the field scattered in the far-field zone of the vacuum as follows [20]:

$$A_{(ba)}^{(1)}(\theta,\varphi) = \sum_{i=1}^{2} K_{i,(ba)}(\alpha,\beta)\hat{a}_i(\alpha - \alpha_0, \beta - \beta_0) \tag{4}$$

The subscript (a) denotes the incident wave polarization (h or v), and the subscript (b) is the scattered wave polarization (h or v). Here, the propagation constants α and β of the scattered wave are defined from the zenith angle θ and azimuth angle φ with $\alpha = k_1 \sin\theta\cos\varphi$ and $\beta = k_1 \sin\theta \sin\varphi$. The first-order scattered amplitudes are expressed as linear combinations of the Fourier transforms $\hat{a}_i(\alpha, \beta)$ of the rough interface height profiles $a_i(x, y)$. The linear combination weights are the first-order SPM kernels. As shown in Appendix A, these kernels depend on the relative permittivity values, the thickness u_0 of the central layer, and the incidence and observation angles.

Within the framework of the first-order SPM and when $L \to +\infty$, the incoherent intensity $I_{f(ba)}^{SPM}(\theta, \varphi)$ is expressed as a linear combination of the spectra of the two rough interfaces [20]:

$$I_{f,(ba)}^{SPM}(\theta,\varphi) = \frac{\cos^2\theta}{\lambda^2 \cos\theta_0} \sum_{i=1}^{2} \left|K_{i(ba)}\right|^2 \hat{R}_{ii}(\alpha - \alpha_0, \beta - \beta_0) \tag{5}$$

Using the first order-SPM kernels, the functional form of first-order SSA model can be obtained [27–31], and the incoherent intensities derived from the SSA approach are found as follows:

$$I^{SSA}_{f,(ba)}(\theta,\varphi) = \frac{\cos^2\theta}{\lambda^2 k_1^2 \cos\theta_0(\cos\theta+\cos\theta_0)^2}\sum_{i=1}^{2}|K_{i,(ba)}|^2\exp[-\sigma_{a_i}^2 k_1^2(\cos\theta+\cos\theta_0)^2]P_i \tag{6}$$

with

$$P_i = \sum_{q=1}^{+\infty}\frac{k_1^{2q}(\cos\theta+\cos\theta_0)^{2q}}{q!}\hat{R}_{ii,q}(\alpha-\alpha_0,\beta-\beta_0) \tag{7}$$

where $R_{ii,q}(x,y) = R^q_{ii}(x,y)$. As shown in Eqs. (6) and (7), the incoherent intensity depends on the rms-heights and on the Fourier transforms of the autocorrelation functions to the power q. For the Gaussian case, the Fourier transforms $\hat{R}_{ii,q}$ are obtained by replacing (l_{xi}, l_{yi}) by $(l_{xi}, l_{yi})/\sqrt{q}$ into Eq. (2), and for the bi-exponential case, by $(l_{xi}, l_{yi})/q$ into Eq. (3), respectively.

For low roughness interfaces, the second-order approximation of $I^{SSA}_{f,(ba)}(\theta,\varphi)$ is equal to $I^{SPM}_{f(ba)}(\theta,\varphi)$. The first-order SPM can be used if the rms-heights of rough surfaces are small compared to the incident wavelength and if the gradients of the surface heights are small compared to 1 [1, 2]. The SSA has a wider validity domain of the SPM and bridges the gap between the SPM and the Kirchhoff Approximation. In [29], we showed that the differences between the backscattered incoherent intensities obtained from the SPM and SSA models increase when increasing the interface roughness and decrease when increasing the incidence angle and that the SSA model can describe the coherent and incoherent intensities for heights twice higher than those obtained by the SPM.

4. INVERSE PROBLEM

4.1. The Cost Function

Our main aim is on retrieving the electrical and geometrical parameters of a stratified medium with two rough interfaces. Complex dielectric constants of the central and lower regions, central layer thickness, root-mean-square height, and correlation lengths of each rough interface are the unknowns in this inverse scattering problem. For the inverse problem, we use synthetic data that are the incoherent intensities obtained from the first-order SSA model, and we use a cost function that consists in the integrated squared deviation between the synthetic data and the incoherent intensities derived from the SPM. We consider mono-frequency bi-static radar configurations. The incoherent intensities are obtained in the incidence plane for several angles of incidence and observation. The cross-polarized incoherent intensities derived from the first-order SPM and first-order SSA vanish in the incidence plane. As a result, we only consider the co-polarized components in the cost function:

$$f_c(\mathbf{x}) = \frac{1}{N_{\theta_0}N_\theta}\sqrt{\sum_{i=1}^{N_{\theta_0}}\sum_{j=1}^{N_\theta}\left[\left(\frac{I^{SPM}_{f,(hh)}(\mathbf{x},\theta_{0i},\theta_j)-I^{(SSA)}_{f,(hh)}(\theta_{0i},\theta_j)}{I^{SSA}_{f,(hh)}(\theta_{0i},\theta_j)}\right)^2+\left(\frac{I^{SPM}_{f,(vv)}(\mathbf{x},\theta_{0i},\theta_j)-I^{(SSA)}_{f,(vv)}(\theta_{0i},\theta_j)}{I^{SSA}_{f,(vv)}(\theta_{0i},\theta_j)}\right)^2\right]} \tag{8}$$

where N_{θ_0} and N_θ are the numbers of incidence and observation angles, respectively. The vector $\mathbf{x}$ contains the unknowns of the inverse problem. In Section 5, we consider snow-covered soils. At L-band frequencies (1–2 GHz), losses in dry snow are known to be very low ($\varepsilon'_{r2} = \mathrm{Re}(\varepsilon_{r2}) \gg \varepsilon''_{r2} = \mathrm{Im}(\varepsilon_{r2}) \approx$ order of 10^{-4}) [35]. As a result, the snow cover is assumed to be a lossless dielectric. For isotropic rough interfaces, the number N of unknowns is equal to 8: ε'_{r2}, ε'_{r3}, ε''_{r3}, u_0, l_1, σ_{a_1}, l_2 and σ_{a_2} where $l_1 = l_{x1} = l_{y1}$ and $l_2 = l_{x2} = l_{y2}$. For anisotropic rough interfaces, $N = 10$ because each autocorrelation function is characterized by two correlation lengths, l_{x1} and l_{y1} for the air-snow interface and l_{x2} and l_{y2} for the snow-soil interface.

4.2. Inversion with a Simulated Annealing Algorithm

The estimation of the electrical and geometrical parameters is obtained from the minimization of the cost function given by Eq. (8). As in [13], the inversion problem is solved using a simulated annealing

(SA) algorithm [22–25]. SA algorithm is one of the most known heuristic methods for solving the optimization problems. The SA algorithm was proposed by Kirkpatrick et al. who were inspired by the metalworking annealing procedure and successfully used in optimization [23, 24]. In general manner, SA algorithm adopts an iterative procedure according to the variable temperature parameter which imitates the annealing transaction of the metal working [23]. The simulated annealing algorithm that we used was developed by Corana et al. [25]. The iteration procedures of simulated annealing algorithms are described in detail in [13] and [23]. The summary of the procedure is illustrated by Appendix B. We recall below the main lines of the process.

First, a set of N_r vectors $\mathbf{x}$ is defined, and the maximum $f_{c,\max}$ of the cost function and the minimum $f_{c,\min}$ are calculated. The initial temperature T_0 is estimated from this set as the ratio $\frac{f_{c,\max}-f_{c,\min}}{N_r}$ (and $T = T_0$). An initial step length vector $\mathbf{v}_0$ is also evaluated as the difference between the lower and upper bounds of $\mathbf{x}$ ($\mathbf{x}_{LB}$ and $\mathbf{x}_{UB}$). Secondly, a random vector $\mathbf{x}_0$ is selected in the feasible region defined by $\mathbf{x}_{LB}$ and $\mathbf{x}_{UB}$, and its cost function $f_c(\mathbf{x}_0)$ is evaluated.

The SA algorithm is a three steps process: perturb the solution, evaluate the quality of the solution, and accept the solution if it is better than the new one. The iteration is given as:

$$x_{new}(m) = x_{old}(m) + rv(m) \tag{9}$$

where $1 \leq m \leq N$. The quantity r is a random number in the range $[-1, 1]$. If this point is outside the study region, the m-th component of $\mathbf{x}$ is adjusted to be there. A new cost function value $f_c(\mathbf{x}_{new})$ is then evaluated. If $f_c(\mathbf{x}_{new}) \leq f_c(\mathbf{x}_{old})$, $\mathbf{x}_{old}$ is replaced by $\mathbf{x}_{new}$ and $f_c(\mathbf{x}_{new})$ is the new minimum. If $f_c(\mathbf{x}_{new}) > f_c(\mathbf{x}_{old})$, the probability $p = e^{-(f_c(\mathbf{x}_{new})-f_c(\mathbf{x}_{old}))/T}$ is evaluated, and a random number $p' \in [0, 1]$ is generated. If $p' < p$, the point of the new step is accepted. Otherwise, it is rejected. This process is for the purpose of reducing the possibility of getting stuck in a local solution, and it is referred to as the Metropolis criterion [13]. The best set of inversion parameters is saved as $\mathbf{x}_{opt}$. N_T loops with the same temperature T are repeated. Each loop consists of N_S cycles where the step length $v(n)$ is adjusted according to the adjustment rule of the Corana algorithm,

$$v_{new}(m) = \begin{cases} \left(1 + \dfrac{n(m)/N_s - 0.6}{0.2}\right) v_{old}(m), & \text{if} \quad n(m) > 0.6N_s \\ \left(1 + \dfrac{0.4 - n(m)/N_s}{0.2}\right)^{-1} v_{old}(m), & \text{if} \quad n(m) < 0.4N_s \\ v_{old}(m), & \text{else} \end{cases} \tag{10}$$

where $1 \leq m \leq N$, and $n(m)$ is the number of accepted moves along the m-th coordinate according to the conditions $f_c(\mathbf{x}_{new}) \leq f_c(\mathbf{x}_{old})$ or $p' < p$. The temperature is then iterated by a reducing factor R_T with $0 < R_T < 1$, and the temperature T is replaced by $\exp(-R_T T)$ in the next iteration of the temperature loop, starting from the current optimum vector.

The process is stopped when the value of the cost function becomes less than a limit value f_{eps}, or when the algorithm converges towards the local minima a certain number of times with a temperature which reaches the minimum $T_{\min} = f_{opt} \cdot 10^{-3}$, or even after a given number N_i of iterations for reasons of computation time.

4.3. SA Algorithm with Noisy Data

The synthetic data are the co-polarized incoherent intensities derived from the SSA. The sensitivity of the inversion scheme to noise on the synthetic data is studied in Section 5. The noise on the reference intensities is assumed to be additive. In small-signal regime, the noisy intensity is modeled as follows:

$$I_{(aa)}^{(NSSA)}(\theta_{0i}, \theta_j) = I_{(aa)}^{(SSA)}(\theta_{0i}, \theta_j) + G\left(0, \sigma_G^2\right) \tag{11}$$

The noise $G(0, \sigma_G^2)$ is assumed to have a Gaussian distribution with zero mean and standard deviation σ_G, and we assume that the standard deviation is proportional to the intensity [13]. Knowing that $G(0, \sigma_G^2) = \sigma_G^2 G(0, 1)$,

$$I_{(aa)}^{(NSSA)}(\theta_{0i}, \theta_j) = (1 + r_0 G(0, 1))\, I_{(aa)}^{(SSA)}(\theta_{0i}, \theta_j) \tag{12}$$

where $G(0,1)$ is a random number with a standard Gaussian distribution, and r_0 is a coefficient of proportionality. We consider several values of r_0, namely: 0.01, 0.025, 0.05, and 0.1. These values correspond to signal to noise ratios (SNRs) of 20, 16, 13, and 10 dB, respectively.

For a set of known parameters $x(m)$ and for each value of r_0, the SA algorithm is run N_n times, and the mean value m_{x_m} and standard deviation σ_{x_m} are derived from the N_n optimized values $x_{opt,j}(m)$ with:

$$m_{x_m} = \frac{1}{N_n}\sum_{j=1}^{N_n} x_{opt,j}(m) \tag{13}$$

$$\sigma_{x_m} = \frac{1}{N_n}\sum_{j=1}^{N_n} \left(x_{opt,j}(m) - m_{x_m}\right)^2 \tag{14}$$

To study the sensitivity of the inversion scheme to noise, we define the relative errors ε_{x_m} between the mean value m_{x_m} and the true value of $x(m)$, and the ratio ρ_{x_m} of the standard deviation σ_{x_m} to the true value of the m-th parameter.

5. INVERSION RESULTS

5.1. Inversion Parameters

For isotropic rough interfaces, the number N of unknowns is equal to 8 and for anisotropic rough interfaces, equal to 10. Table 1 gives the electrical and geometrical parameters, the true values of these parameters, and the lower and upper bounds of $\mathbf{x}$ ($\mathbf{x}_{LB}$ and $\mathbf{x}_{UB}$) for the isotropic configurations and Table 2, for anisotropic ones. In fact, for the anisotropic configurations, the lower rough interface is isotropic, but we do not make the assumption a priori that this interface is isotropic.

Table 1. True values of the electrical and geometrical parameters, lower and upper bounds of the parameter vector for the isotropic configurations. The geometrical parameters ($4 \leq m \leq 8$) are expressed in cm.

Parameters	ε'_{r1}	ε'_{r2}	ε''_{r2}	u_0	l_1	σ_{a1}	l_2	σ_{a2}
m	1	2	3	4	5	6	7	8
x_{LB} (m)	1.5	10	1.00	0	2	0	5	0
x_{UB} (m)	4.0	25	5	30	10	2	20	2
True values	3	20	2.55	10	6	0.5	9	0.7

Table 2. True values of the electrical and geometrical parameters, lower and upper bounds of the parameter vector for the anisotropic configurations. The geometrical parameters ($4 \leq m \leq 10$) are expressed in cm.

Parameters	ε'_{r1}	ε'_{r2}	ε''_{r2}	u_0	l_{x1}	l_{y1}	σ_{a1}	l_{x2}	l_{y2}	σ_{a2}
m	1	2	3	4	5	6	7	8	9	10
$x_{LB}(m)$	1.5	10	1.00	0	2	8	0	5	5	0
$x_{UB}(m)$	4.0	25	5	30	10	16	2	20	20	2
True values	3	20.5	2.55	10	6	12	0.5	9	9	0.7

The values of N_S, N_T, and R_T used in this study are those recommended by Corana et al. [25], i.e., 20, 100, and 0.85, respectively. The value of T_0 is obtained by taking $N_r = 2000$. The number of iterations N_i, the limit f_{eps} of the cost function, and the final temperature T_{fin} are empirically derived. We take $f_{eps} = 5 \times 10^{-5}$, $T_{fin} = 10^{-5}$, and $N_i = 200$. The mean value m_{x_m}, standard deviation

σ_{x_m}, relative errors ε_{x_m} between the mean value m_{x_m} and the ratio ρ_{x_m} are derived from a set of N_n estimated vectors $\mathbf{x}_{opt}$ with $N_n = 40$.

5.2. Isotropic Configurations — An Eight-Parameter Problem

We consider a snow-covered soil illuminated by an h- or v-polarized plane wave of wavelength $\lambda = 30\,\text{cm}$. The rough interfaces are characterized by Gaussian or bi-exponential correlation functions. The true values of electrical and geometrical parameters are given in Table 1. We must deal with an 8-parameter inversion problem. We consider four configurations. The synthetic co-polarized intensities are obtained with the SSA model in the incidence plane $\varphi = \varphi_0 = 0°$.

- For configurations C1, the autocorrelation function is Gaussian. We choose the incidence angles to be $\theta_0 = 30°$ and $\theta_0 = 60°$ and the observation angles θ ranging from $-60°$ to $+60°$ in steps of $15°$. We therefore seek to estimate 8 parameters from a cost function that uses 18 incoherent intensity values.
- For the configurations C2, the autocorrelation function is also Gaussian, but the incidence angle θ_0 varies from $15°$ to $60°$ in steps of $15°$ and the observation angle θ, from $-60°$ to $+60°$. We want to estimate 8 parameters from a cost function that uses 36 incoherent intensity values.
- For configurations C3 and C4, the autocorrelation function is a bi-exponential function, and the incidence and observation angles are those of configurations C1 and C2.

We analyze the sensitivity of the inversion algorithm to noise with r_0 equal to 0.01, 0.025, 0.05, and 0.1. For a given value of r_0, the SA algorithm is used 40 times to estimate the 8 parameters with 40 different sets of 18 or 36 incoherent intensities obtained from the SSA model.

Figures 2 and 3 show the relative errors ε_{x_m} (in percent) as a function of r_0. The inversion problem is fully optimized when the optimized value of each parameter is equal to its actual value. But in this case, the values of the intensities derived from the SSA method are different from those obtained from the SPM, and therefore in the absence of noise ($r_0 = 0$), the relative errors are not equal to zero. Except

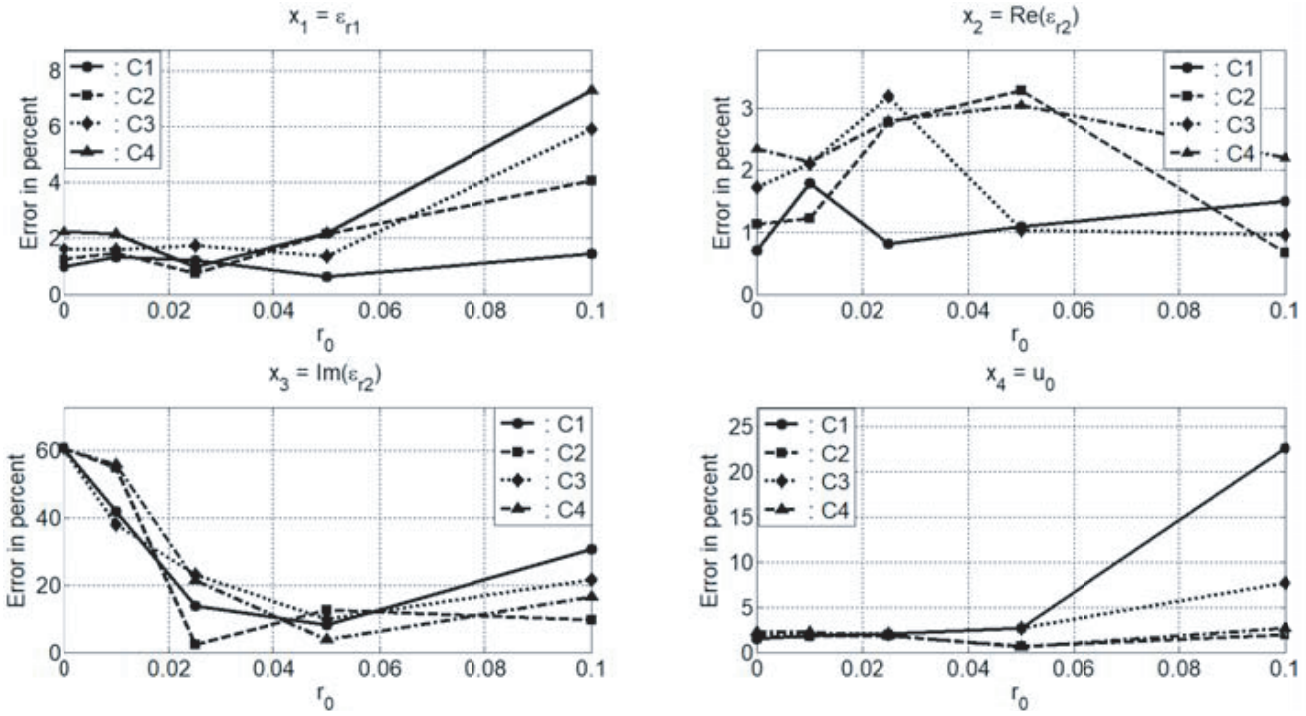

Figure 2. Relative errors (in percent) on the electrical parameters and the snow-cover thickness — Isotropic configurations.

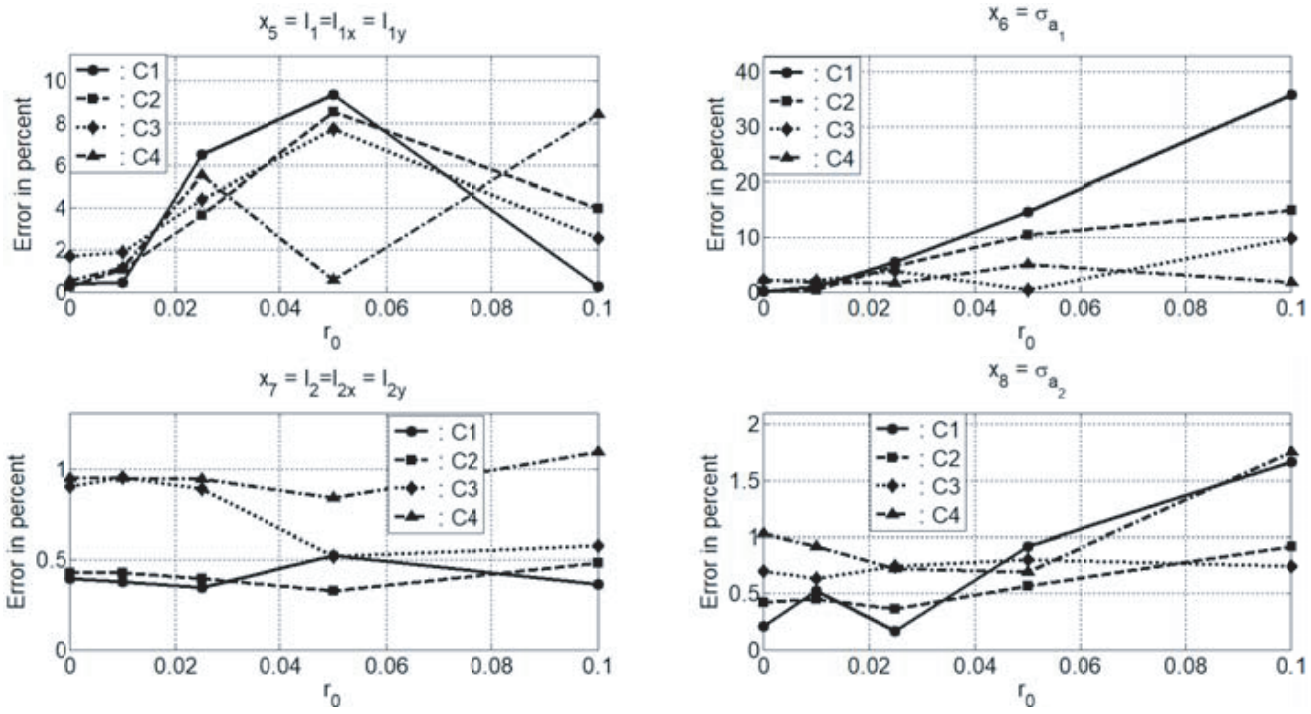

Figure 3. Relative errors (in percent) on the roughness parameters — Isotropic configurations.

for the imaginary part of the complex permittivity of the soil, we find that the relative errors made are low when $r_0 = 0$.

For all values of r_0, these errors are less than 10 per cent for the snow permittivity, for the real part of the soil permittivity, for the roughness parameters of the snow/soil interface, and for the correlation length of the air/snow interface. For configurations C1 and C3, the relative errors made on the rms-height of the air/snow interface are greater than 10% for $r_0 \geq 0.05$, and for configurations C1, the relative error made on the thickness of the layer of snow is greater than 10% when $r_0 = 0.1$. The estimation technique is biased, but committed relative errors are less than 10% in 82.5% of treated cases for configurations C1, 87.50% for C2 and C3, 90% for C4. In light of the results presented, we can conclude that the noise resistance of the inversion scheme is good on average.

The highest relative error is made on the parameter x_3 that is the imaginary part ε''_{r2}. We can nevertheless see that the error decreases when r_0 increases from 0 to 0.05 and then increases when r_0 is greater than 0.05. For all configurations, the relative error on this parameter is minimal at $r_0 = 0.05$. This behavior is also observed (less markedly) for parameter x_4 which corresponds to the thickness of the snow cover. In the presence of a noise defined by $r_0 = 0.025$ or 0.05, the relative error made on each of the parameters is less than 10%. The intensities obtained with the SPM used with the actual values of parameters underestimate the values obtained with the SSA method. For certain values of the signal-to-noise ratio, the additive noise reduces the quadric distance between the intensity curves obtained with the two analytical models and allows better results to be obtained. For $r_0 = 0.05$, the noise has a beneficial effect for the determination of the parameters.

Increasing the number of data (from 18 to 36) does not significantly reduce errors. The errors made for configurations C1 and C3 are greater than those made for configurations C2 and C4, in 50% of treated cases. In 70% of treated cases, the errors obtained with the bi-exponential function (C3 and C4 configurations) are larger than those obtained with the Gaussian one (Configurations C1 and C2).

Figures 4 and 5 show the ratios ρ_{x_m} as a function of r_0. These ratios increase with r_0 because of the greater variability of inverse problem results when the signal-to-noise ratio decreases. Increasing the number of data (from 18 to 36) does reduce the variability. The ratio values obtained for configurations C1 and C3 are greater than those made for configurations C2 and C4 in 80% of treated cases. Performance depends on the shape of the correlation function. It is better in the case of the Gaussian

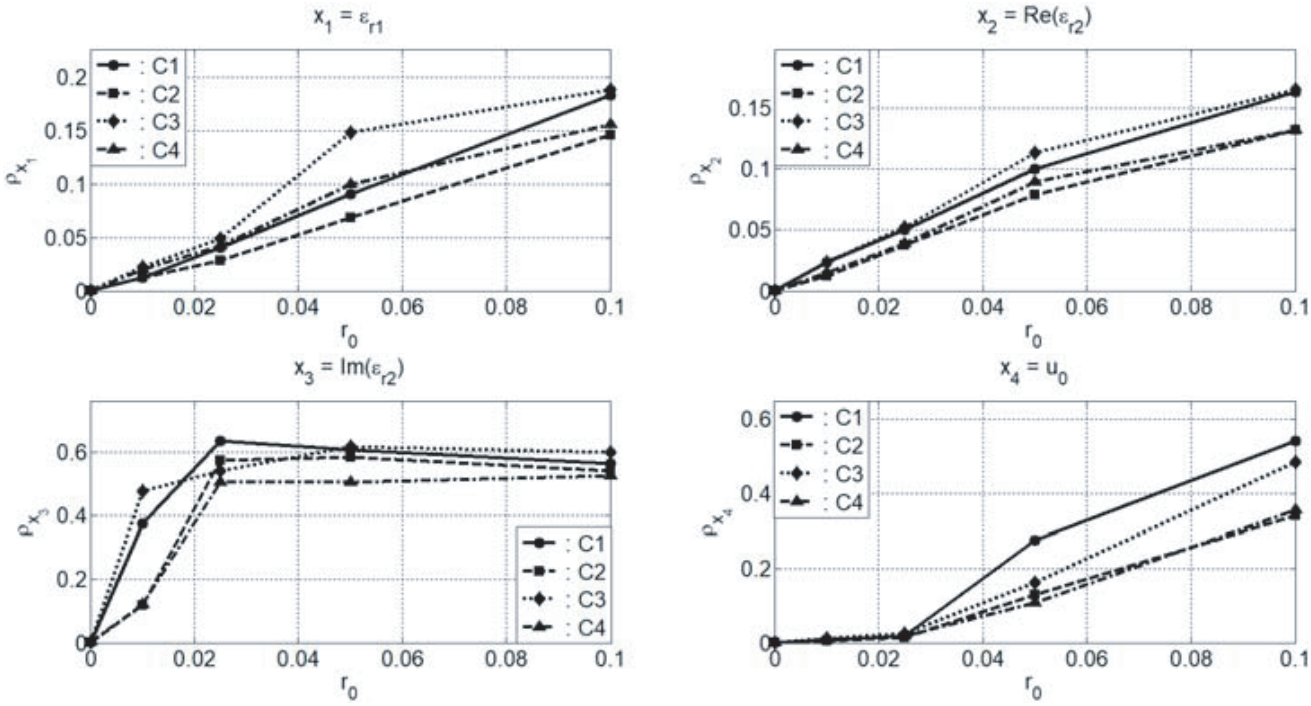

Figure 4. Ratios ρ_{x_m} for the electrical parameters and the snow-cover thickness — Isotropic configurations.

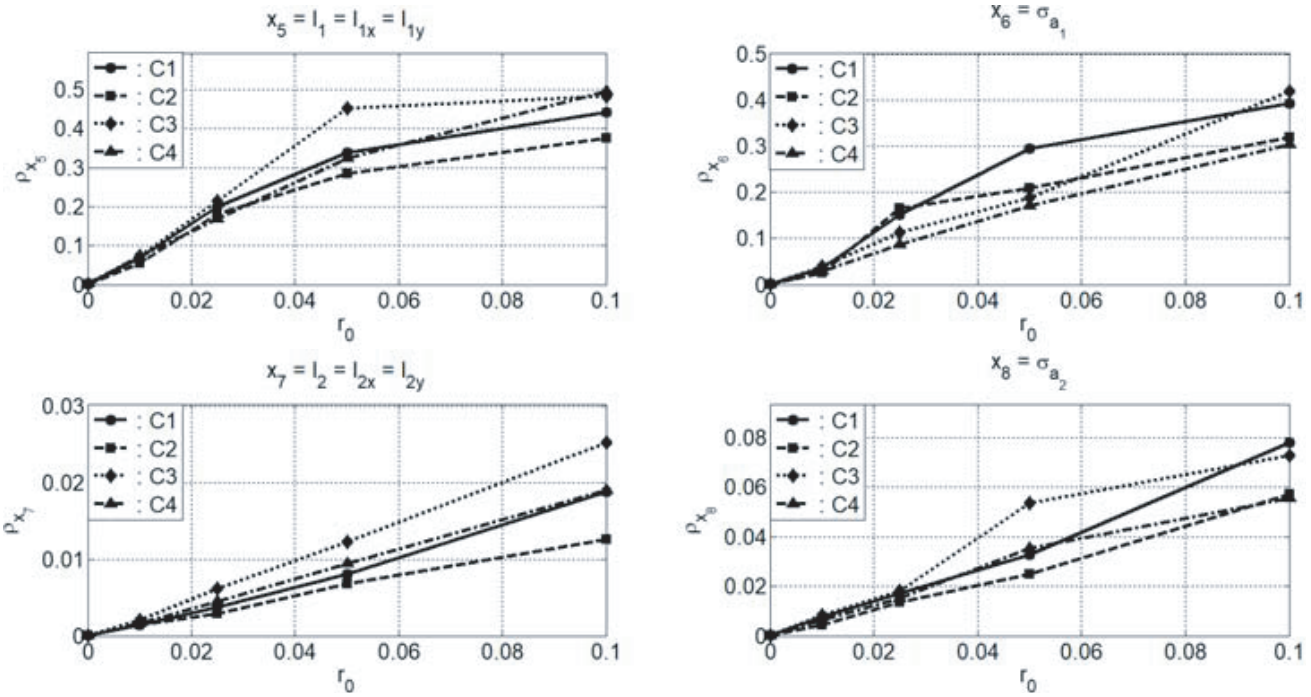

Figure 5. Ratios ρ_{x_m} for the roughness parameters – Isotropic configurations.

function. In 80% of treated cases, the ratios obtained with the bi-exponential function (C3 and C4 configurations) are larger than those obtained with the Gaussian one (Configurations C1 and C2). When $r_0 \leq 0.025$, the ratio ρ_{x_m} is less than 10% for five of the eight parameters: for the snow permittivity,

for the real part of the soil permittivity, and for the roughness parameters of the snow/soil interface. The variability is greater on the roughness parameters of the air/snow interface. The values of ρ_{x_5} and ρ_{x_6} are lower than 10% for $r_0 = 0.01$.

5.3. Anisotropic Configurations — A Ten-Parameter Problem

The autocorrelation function of the air/snow interface is anisotropic. The correlation length l_{x1} is equal to 6 cm and the correlation length l_{y1} to 12 cm. The values of the electric parameters and those of the other geometrical parameters are unchanged compared to the isotropic configurations. Nevertheless, we do not make the assumption a priori that the snow/soil interface is isotropic. We must deal with a 10-parameter inversion problem. First, we have analyzed configurations C2 and C4 for which the autocorrelation function is a Gaussian function and a bi-exponential function, respectively, for which the incidence angle θ_0 varies from 15° to 60° in steps of 15°, observation angle θ, from −60° to +60°, and $\varphi = \varphi_0 = 0°$. The inversion algorithm does not allow the two correlation lengths of the snow/soil interface to be determined. To determine the two correlation lengths of this isotropic interface, we must take into account information in several incidence planes $\varphi = \varphi_0$, i.e., for several values of azimuth angles φ_0. We then consider two new configurations.

- For configurations C5, the autocorrelation function is Gaussian. The co-polarized incoherent intensity values are obtained in the incidence plane $\varphi = \varphi_0 = 15°$ under the incidence angles $\theta_0 = 15°$ and also, in the incidence plane $\varphi = \varphi_0 = 45°$ under the incidence angles $\theta_0 = 30°$ and $\theta_0 = 60°$. The observation angles θ range from −60° to +60° in steps of 15°. We therefore seek to estimate 10 parameters from a cost function that uses 36 incoherent intensity values.
- For configurations C6, the autocorrelation function is a bi-exponential function, and the angles are those of configurations C5.

Figures 6 and 7 show the relative errors ε_{x_m} (in percent) as a function of r_0. As for isotropic cases and except for the imaginary part of the complex permittivity of the soil, the relative errors made are

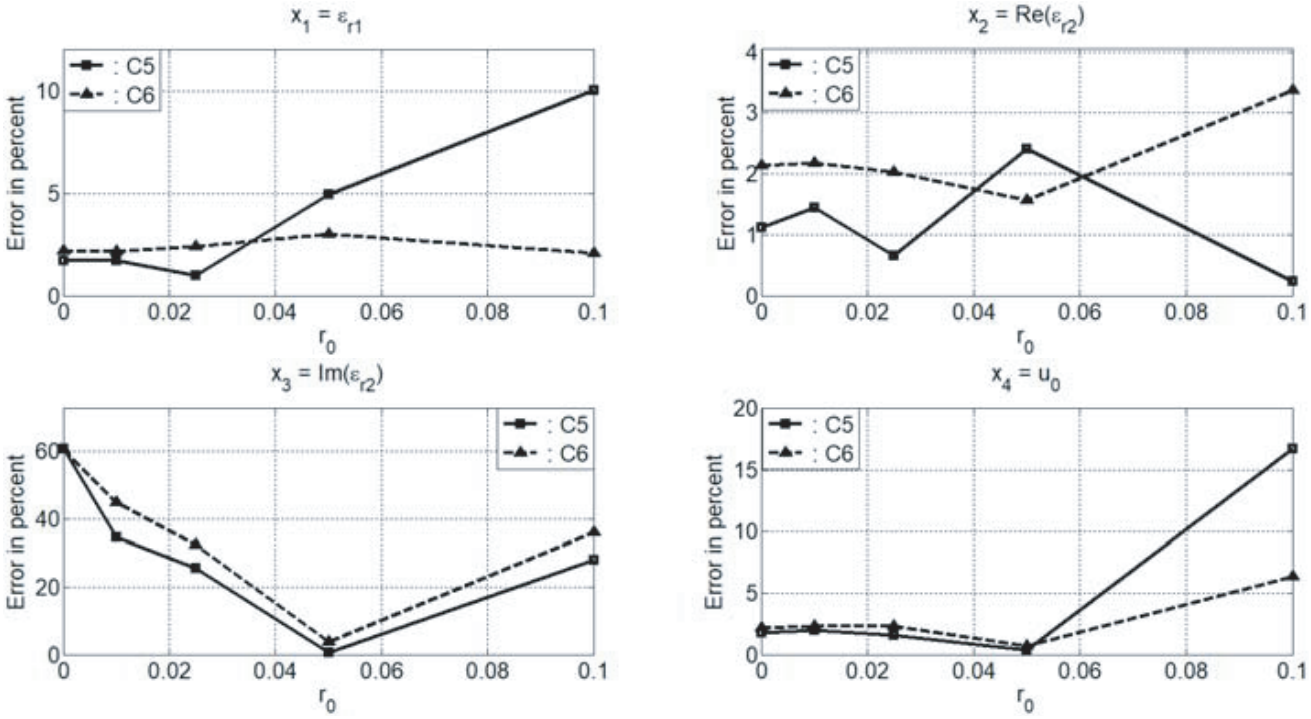

Figure 6. Relative errors (in percent) on the electrical parameters and the snow-cover thickness — Anisotropic configurations.

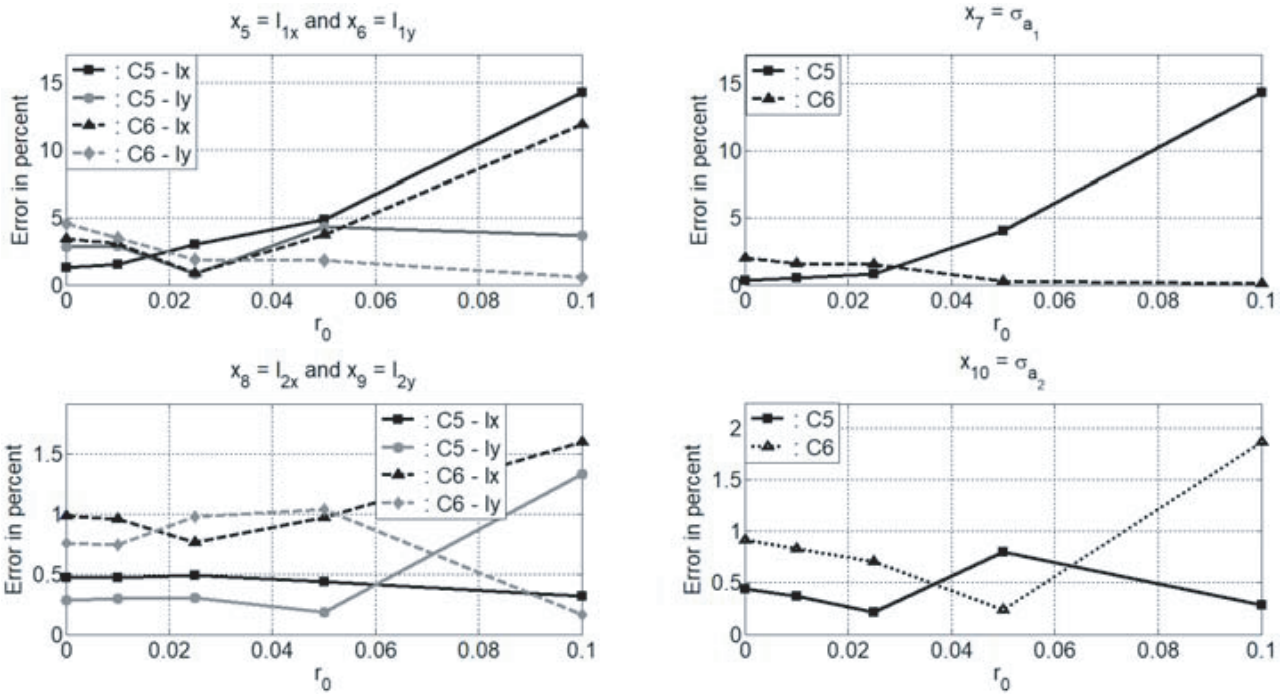

Figure 7. Relative errors (in percent) on the roughness parameters — Anisotropic configurations.

small when $r_0 = 0$. For parameters x_3 and x_4, the relative errors decrease when r_0 increases from 0 to 0.05 and then increase when r_0 is greater than 0.05. In the presence of a noise defined by $r_0 = 0.05$, the relative error made on each of the parameters is less than 10%, and the noise with $r_0 = 0.05$ has a beneficial effect upon the inversion problem.

For all values of r_0, these errors are less than 10 per cent for the snow permittivity, for the real part of the soil permittivity, for the snow-cover thickness, and for the roughness parameters of the snow/soil interface. For configurations C5, the relative error made on the rms-height of the air/snow interface is greater than 10% when $r_0 > 0.05$ and for configurations C6, and the relative error is always less than 10%. For both the configurations C5 and C6, the relative error made on the correlation length along the Oy axis is less than 10%. The error on the correlation length l_x is greater than 10% when $r_0 > 0.05$. The estimation technique is biased, but committed relative errors are less than 10% in 84% of treated C5-cases and in 90% of C6-cases. As previously shown, in light of the results presented, we can conclude that the noise resistance of the inversion scheme is good on average. In 72% of treated cases, the errors obtained with the bi-exponential function (C6 configurations) are larger than those obtained with the Gaussian one (Configurations C5).

Table 3 gives the mean value for the four correlation lengths in the case of Gaussian autocorrelation functions. Table 4 gives results in the bi-exponential case. The biases on the correlation lengths are

Table 3. Mean values of correlation lengths estimated over 40 realizations. Anisotropic configurations — Gaussian case (C5).

r_0	0	0.01	0.025	0.05	0.1
$m_{l_{x1}}$ in cm	6.08	6.09	6.18	5.77	5.15
$m_{l_{y1}}$ in cm	11.7	11.7	11.9	11.5	11.6
$m_{l_{x2}}$ in cm	8.96	8.96	8.96	8.96	8.97
$m_{l_{y2}}$ in cm	8.97	8.97	8.97	8.98	8.88

Table 4. Mean values of correlation lengths estimated over 40 realizations. Anisotropic configurations — Bi-exponential case (C6).

r_0	0	0.01	0.025	0.05	0.1
$m_{l_{x1}}$ in cm	6.20	6.18	6.05	6.22	6.71
$m_{l_{y1}}$ in cm	11.45	11.6	11.8	11.8	11.9
$m_{l_{x2}}$ in cm	8.91	8.91	8.93	8.91	8.86
$m_{l_{y2}}$ in cm	8.93	8.93	8.91	8.91	8.99

low. We find in particular the two correlation lengths of the second interface which is isotropic. These correlation lengths are almost equal whatever the SNR value is.

Figures 8 and 9 show the ratios ρ_{x_m} as a function of r_0. These ratios increase with r_0 because of the greater variability of inverse problem results when the signal-to-noise ratio decreases. These ratios are less than 10% in 68% of the cases treated for all the C5 and C6 configurations. When $r_0 \leq 0.025$, the ratio ρ_{x_m} of the standard deviation σ_{x_m} to the true value of the m-th parameter are less than 10% for six of the ten parameters: for the snow permittivity, for the real part of the soil permittivity, for the roughness parameters of the snow/soil interface, and for the rms-height of the air/snow interface. The variability is greater on both the correlation lengths of the upper interface. The values of ρ_{x_5} and ρ_{x_6} are lower than 10% for $r_0 = 0.01$. As previously shown, performance depends on the shape of the correlation function. They are better in the case of Gaussian functions. In 76% of treated cases, the ratios obtained with the bi-exponential function (Configurations C6) are larger than those obtained with the Gaussian one (C5). In view of the results presented, we obtain performances similar to those obtained with the isotropic configurations, but the inversion requires to have data in several planes of incidence.

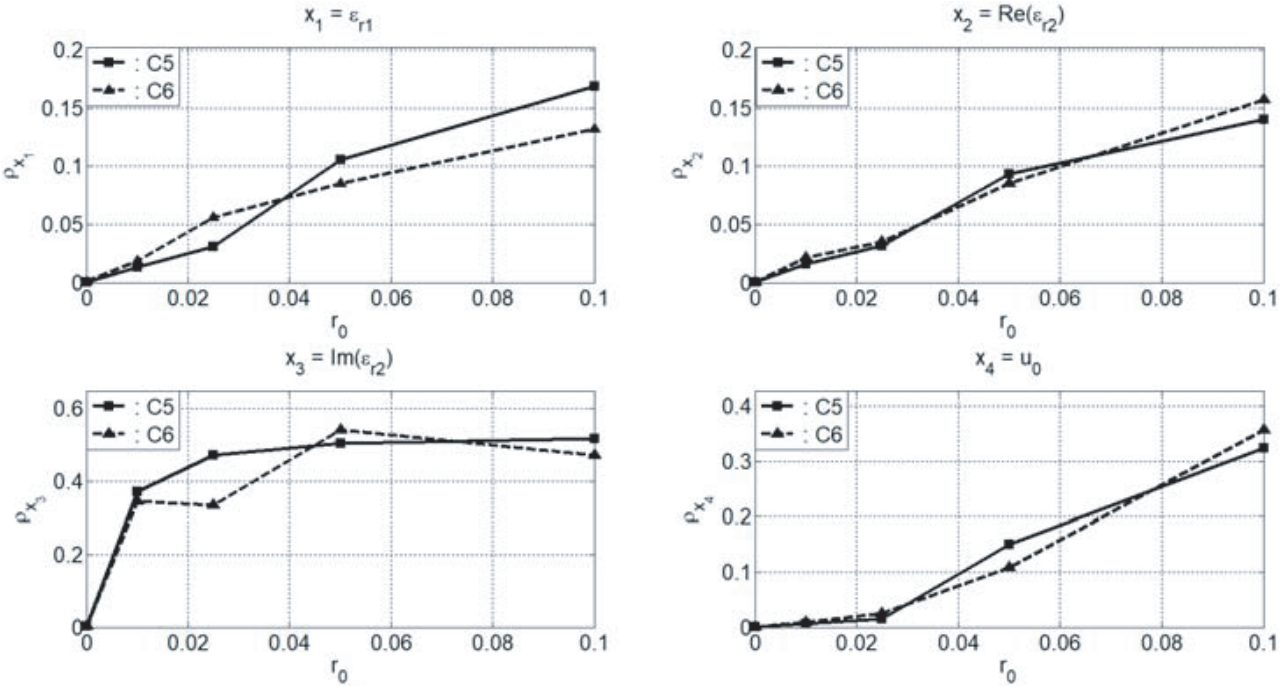

Figure 8. Ratios ρ_{x_m} for the electrical parameters and the snow-cover thickness — Anisotropic configurations.

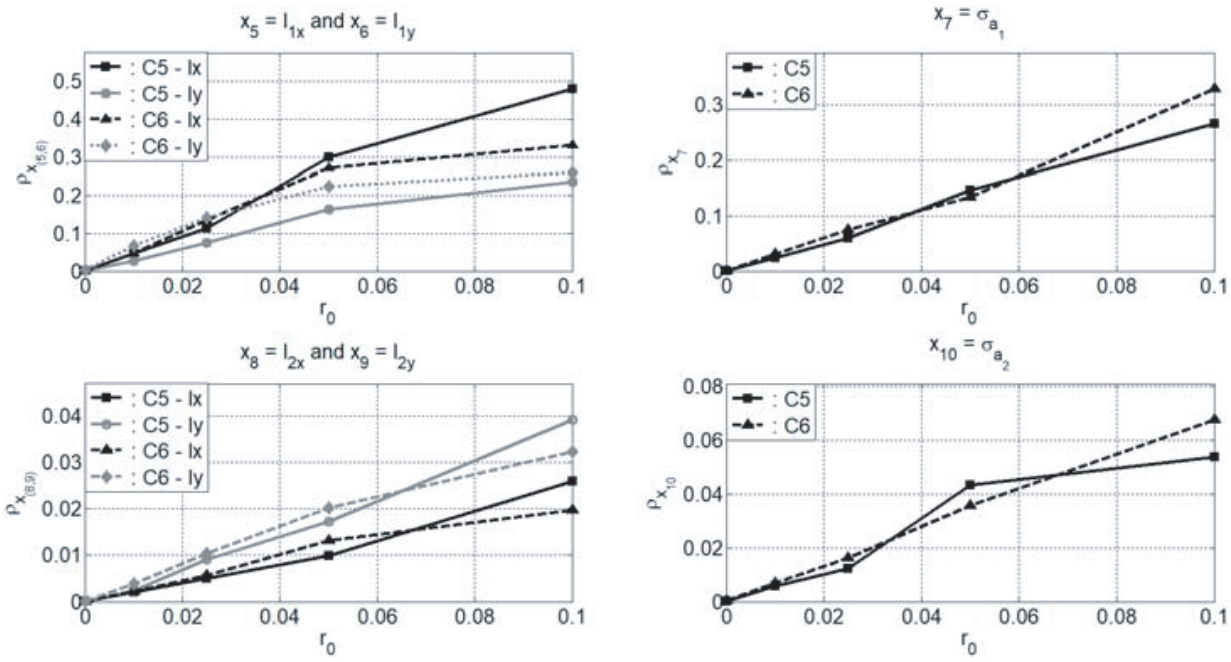

Figure 9. Ratios ρ_{x_m} for the roughness parameters — Anisotropic configurations.

5.4. Snow Cover Thickness Estimation

Figure 10 shows the optimized value of the snow cover thickness as a function of the true value in the case of Gaussian autocorrelation function. Figure 11 shows the curves with the bi-exponential function. The true value of the thickness varies from 5 cm to 50 cm in steps of 5 cm, and the other model parameters are those of configurations C5 and C6. For a given value of r_0, each point of the curve is obtained from

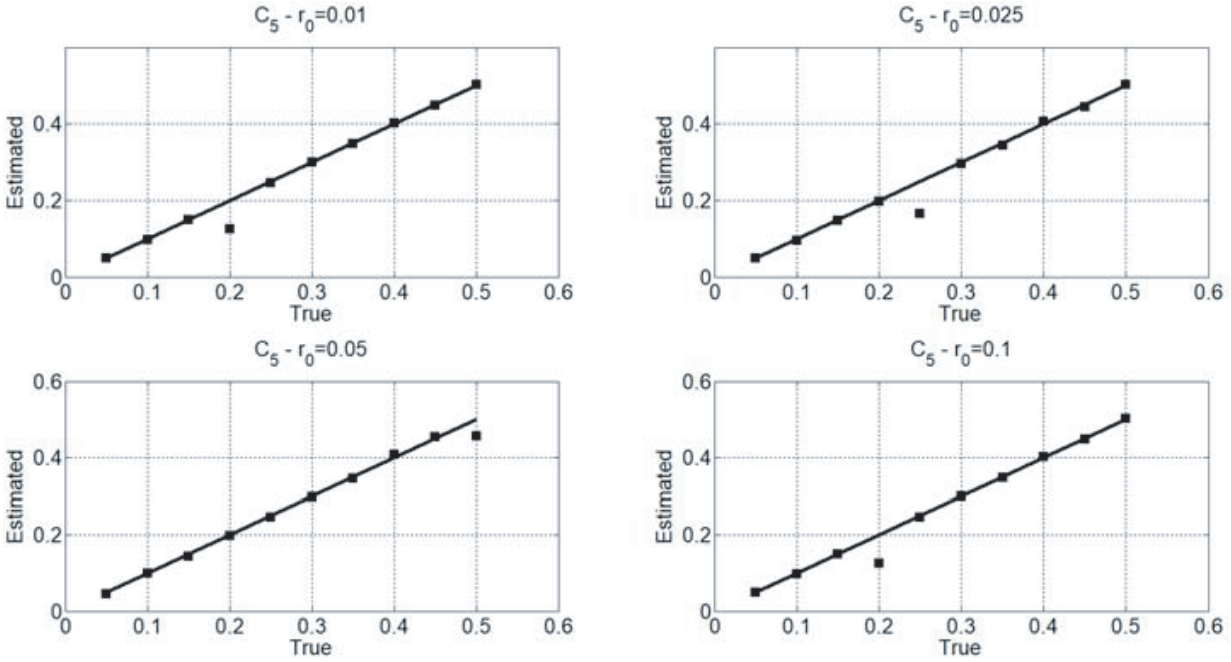

Figure 10. Value of thickness of the snow cover estimated from a set of noisy incoherent intensities as a function of the actual thickness for the C5 configurations (Gaussian autocorrelation function — Anisotropic case).

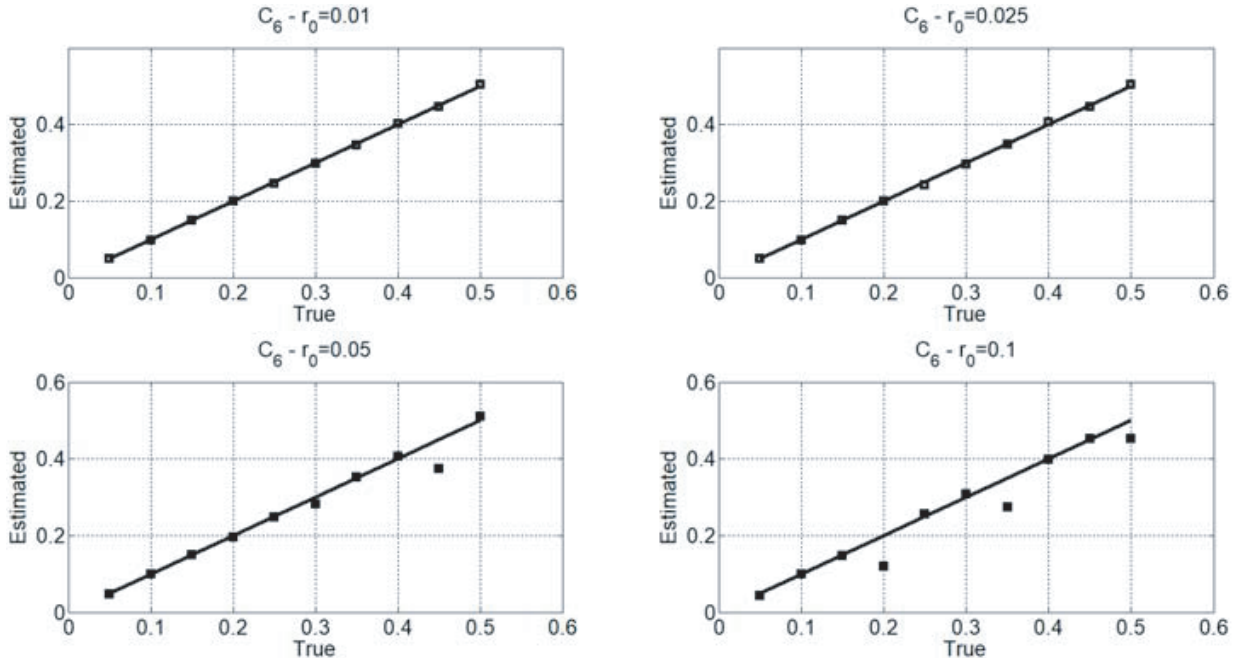

Figure 11. Value of thickness of the snow cover estimated from a set of noisy incoherent intensities as a function of the true value for the C6 configurations (bi-exponential autocorrelation function — Anisotropic case).

a single set of 36 values of the incoherent intensity perturbed by an additive noise. These two figures show that the noise resistance remains good even if the thickness is changed. In the Gaussian case, the inversion algorithm provides conclusive results for 37 of the 40 simulation points. For bi-exponential autocorrelation functions, the SA algorithm gives conclusive estimations for 36 of the 40 simulations points. Three of the 4 points where the relative error is greater than 10% are on the curve obtained for $r_0 = 0.1$. A way to improve the accuracy of inversion is to average several noisy-data points and use the averaged data into the SA algorithm.

6. CONCLUSION

We have presented the application of the simulated annealing algorithm to the inversion of the model parameters characterizing a stratified structure with two rough interfaces. The inversion scheme is applied to the electrical and geometrical parameters involved into the formulae giving the co-polarized incoherent intensities with the SPM. The synthetic data are the co-polarized incoherent intensities obtained from the first-order Small Slope Approximation. The cost function consists in the integrated squared deviation between the incoherent intensities obtained from the Small Slope Approximation and those obtained from the Small Perturbation Method. We consider mono-frequency bi-static radar configurations and incoherent intensity values obtained from several incidence and observation angles.

The capability of other inversion methods such as particle swarm [37] or genetic algorithm [38, 39] can be studied for the purpose of subsurface characterization. It would be interesting to conduct a comparative study to define the potential of each of the methods. Such a comparative study is beyond the scope of this paper. Nevertheless, before using the simulated annealing method, we used the particle swarm optimization. We have observed that the SA method is more efficient and gives good results with a better resistance to noise and a shorter computational time. In particular, the SA method is more efficient for estimating geometrical parameters.

We have studied the sensitivity of the inversion scheme to noise on the synthetic data and the influence of the shape of the autocorrelation function upon the estimation of parameters. We consider bi-exponential and Gaussian functions. We have also analysed configurations for which the autocorrelation

of the upper rough interface is anisotropic and characterized by two correlation lengths. The study is applied to snow-covered soils in L-band. For isotropic rough interfaces, the number of unknowns is equal to 8 and for anisotropic rough interfaces, equal to 10. For a set of known parameters and for several values of signal to noise ratios, the SA algorithm is run N_n times, and the mean value and standard deviation are derived from the N_n optimized values of each electrical or geometrical parameter. To study the sensitivity of the inversion scheme to noise, we define the relative errors ε_{x_m} between the mean value and the true value of the parameter and the ratio ρ_{x_m} of the standard deviation to the true value. We show that the estimation technique is biased, but the noise resistance of the inversion scheme is good on average for the isotropic configurations. When the signal-to-noise ratio decreases, the variability of inverse problem results and the ratios ρ_{x_m} increase. Increasing the number of data (from 18 values of the incoherent intensity to 36) does not significantly reduce relative errors. On the other hand, increasing the number of data does reduce the variability. Performance depends on the shape of the correlation function. It is better in the case of Gaussian functions. We draw the same conclusions for anisotropic configurations, but to determine all the correlation lengths, we must take into account information in incidence planes defined by different azimuth angles. We show that the noise resistance remains good whatever the snow-cover thickness and the inversion method is efficient for estimating this geometrical parameter.

APPENDIX A. EXPRESSIONS OF THE FIRST-ORDER SPM KERNELS

For an incident wave of horizontal polarization, the first-order Kernels $K_{i,(hh)}(\alpha,\beta)$ and $K_{i,(vh)}(\alpha,\beta)$ of the SPM associated with the progressive plane waves scattered in the region 1 are expressed in the following forms [20]:

$$\begin{aligned} K_{1(hh)} &= j2\gamma_{10}\frac{(k_1^2-k_2^2)\cos(\varphi-\varphi_0)}{r_{oh}r_h(\gamma)} \\ &\quad\times[\gamma_2\cos(\gamma_2u_0)+j\gamma_3\sin(\gamma_2u_0)][\gamma_{20}\cos(\gamma_2u_0)+j\gamma_{30}\sin(\gamma_2u_0)] \qquad \text{(A1)} \\ K_{2(hh)} &= j2\gamma_{10}\frac{(k_2^2-k_3^2)\gamma_2\gamma_{20}}{r_{oh}r_h(\gamma)}\cos(\varphi-\varphi_0) \qquad \text{(A2)} \\ K_{1(vh)} &= j2\gamma_{10}\frac{(k_1^2-k_2^2)k_1\gamma_2\sin(\varphi-\varphi_0)}{r_{oh}r_v(\gamma)} \\ &\quad\times[k_2^2\gamma_3\cos(\gamma_2u_0)+jk_3^2\gamma_2\sin(\gamma_2u_0)][\gamma_{20}\cos(\gamma_{20}u_0)+j\gamma_{30}\sin(\gamma_{20}u_0)] \qquad \text{(A3)} \\ K_{2(vh)} &= j2\gamma_{10}\frac{(k_2^2-k_3^2)k_1k_2^2\gamma_{20}\gamma_2\gamma_3}{r_{oh}r_v(\gamma)}\sin(\varphi-\varphi_0) \qquad \text{(A4)} \end{aligned}$$

with

$$r_h(\gamma)=\gamma_2(\gamma_1+\gamma_3)\cos(\gamma_2u_0)+j(\gamma_2^2+\gamma_1\gamma_3)\sin(\gamma_2u_0) \qquad \text{(A5)}$$

The propagation constants γ_i $(i=1,2,3)$ have an imaginary part less than or equal to zero with $\gamma_i^2+\beta^2+\alpha^2=k_i^2$ $(\mathrm{Im}(\gamma_i)\le 0)$. The propagation constants γ_i associated with (α_0,β_0) are denoted as $\gamma_{i0}=\gamma_i(\alpha_0,\beta_0)$ and $r_{0h}=r_h(\alpha_0,\beta_0)$. For a progressive plane wave travelling without attenuation in region 1, $\gamma_1=k_1\cos\theta$.

For an incident wave of vertical polarization, the complex amplitudes $K_{i,(vv)}(\alpha,\beta)$ and $K_{i,(hv)}(\alpha,\beta)$ have the following expressions:

$$\begin{aligned} K_{1vv} &= j2\gamma_{10}\frac{\left(k_1^2-k_2^2\right)}{r_{ov}r_v(\gamma)}\left\{k_2^2\chi\chi_0\left[k_3^2\gamma_2\cos\left(\gamma_2u_0\right)+jk_2^2\gamma_3\sin\left(\gamma_2u_0\right)\right]\right. \\ &\quad\times\left[k_3^2\gamma_{20}\cos\left(\gamma_{20}u_0\right)+jk_2^2\gamma_{30}\sin\left(\gamma_{20}u_0\right)\right]-k_1^2\gamma_2\gamma_{20}\cos\left(\varphi-\varphi_0\right) \\ &\quad\left.\times\left[k_2^2\gamma_3\cos\left(\gamma_2u_0\right)+jk_3^2\gamma_2\sin\left(\gamma_2u_0\right)\right]\left[k_2^2\gamma_{30}\cos\left(\gamma_{20}u_0\right)+jk_3^2\gamma_{20}\sin\left(\gamma_{20}u_0\right)\right]\right\} \qquad \text{(A6)} \\ K_{2vv} &= j2\gamma_{10}\frac{\left(k_2^2-k_3^2\right)k_1^2k_2^2\gamma_{20}\gamma_2}{r_{ov}r_v(\gamma)}\left[k_3^2\chi\chi_0-k_2^2\gamma_{30}\gamma_3\cos\left(\varphi-\varphi_0\right)\right] \qquad \text{(A7)} \end{aligned}$$

$$K_{1hv} = j2\gamma_{10}\frac{\left(k_1^2-k_2^2\right)k_1\gamma_{20}\sin\left(\varphi-\varphi_0\right)}{r_{ov}r_v(\gamma)} \times\left[k_2^2\gamma_{30}\cos\left(\gamma_{20}u_0\right)+jk_3^2\gamma_{20}\sin\left(\gamma_{20}u_0\right)\right]\left[\gamma_2\cos\left(\gamma_2u_0\right)+j\gamma_3\sin\left(\gamma_2u_0\right)\right] \quad \text{(A8)}$$

$$K_{2hv} = j2\gamma_{10}\frac{\left(k_2^2-k_3^2\right)k_1k_2^2\gamma_{20}\gamma_2\gamma_{30}}{r_{ov}r_h(\gamma)}\sin\left(\varphi-\varphi_0\right) \quad \text{(A9)}$$

with

$$r_v(\gamma)=k_2^2\gamma_2\left(k_3^2\gamma_1+k_1^2\gamma_3\right)\cos\left(\gamma_2u_0\right)+j\left(k_1^2k_3^2\gamma_2^2+k_2^4\gamma_1\gamma_3\right)\sin\left(\gamma_2u_0\right) \quad \text{(A10)}$$

and $r_{0v}=r_v(\alpha_0,\beta_0)$, $\chi=\sqrt{\alpha^2+\beta^2}$ and $\chi_0=\sqrt{\alpha_0^2+\beta_0^2}$.

When the denominator of first-order Kernel vanishes (i.e., when $r_{0a}=0$ or $r_b=0$), a resonance phenomenon occurs. Insofar as the propagation constants γ_{30} and γ_3 are complex and taking into account the incidence and observation angles used in our study, the resonance phenomenon does not occur regardless of the thickness of the snow cover.

APPENDIX B. SIMULATED ANNEALING ALGORITHM

Data : N , N_S , N_T , R_T , $feps$, x_{LB} , x_{UB}
Results : x_{opt} , f_{opt}
Initialization:
$x_0 = x_{LB} + rand(N,1).(x_{UB} - x_{LB})$; $v_0 = x_{UB} - x_{LB}$
$T_0 = (f_{c,\max} - f_{c,\min}) / N_r$
$f = f_c(x_0)$; $f_{opt} = f = f_c(x_0)$
while $f_{opt} > f_{eps}$ do
  while $T > f_{eps}.10^{-3}$ do
    $v = v_0$;
    for $nt = 1$ to N_T do {Loop temperature reduction tests}
      $ncont = 0$;
      for $j = 1$ to N_S do {Loop on step variation tests}
        for $m = 1$ to N do {Generate and test for each parameter}
          $x'(m) = x(m) + rv(m)$
          if $x'(m) < x_{LB}(m)$ or $x'(m) > x_{UB}(m)$ then generate a new trial point
          else Calculate $f_c(x')$
            Generate a random $x' \in [0,1]$
            if $f_c(x') < f_c(x)$ or $p' < e^{-(f_c(p')-f_c(p))/T}$
              $x = x'$; $f_c(x) = f_c(x')$;
              if $f_c(x') < f_{opt}$
                $x_{opt} = x'$; $f_{opt} = f_c(x')$; $ncont(m)++$ {count the number of accepted case}
              end if
            end if
        end for
      end for
      Adjust the step length for each parameter $v(m)$
    end for
    if $f_{opt} < f_{eps}$ STOP
    else $T \leftarrow T.\exp(-R_T)$ {Reduce temperature}
  end while
  if $f_{opt} < f_{eps}$ STOP
  else $T \leftarrow 1000 * T$ {Increase the temperature}
end while

REFERENCES

1. Tabatabaeenejad, A. and M. Moghaddam, "Study of validity region of small perturbation method for two-layer rough surfaces," *IEEE Geosci. Remote Sens. Lett.*, Vol. 7, No. 2, 319–323, Apr. 2010.
2. Imperatore, P., A. Iodice, M. Pastorino, and N. Pinel, "Modelling scattering of electromagnetic waves in layered media: An up-to-date perspective," *Int. J. Antennas Propag.*, Vol. 2017, 1–14, 2017.
3. Amra, C., M. Lequime, and M. Zerrad, *Electromagnetic Optics of Thin-film Coatings: Light Scattering, Giant Field Enhancement, and Planar Microcavities*, Cambridge University Press, 2021.
4. El-Shenawee, M., "Polarimetric scattering from two-layered two dimensional random rough surfaces with and without buried objects," *IEEE Trans. Geosci. Remote Sens.*, Vol. 42, No. 1, 67–76, Jan. 2001.
5. Déchamps, N., N. de Beaucoudrey, C. Bourlier, and S. Toutain, "Fast numerical method for electromagnetic scattering by rough layered interfaces: Propagation-inside-layer expansion method," *J. Opt. Soc. Amer. A*, Vol. 23, No. 2, 359, Feb. 2006.
6. Déchamps, N. and C. Bourlier, "Electromagnetic scattering from a rough layer: Propagation-inside-layer expansion method combined to the forward-backward novel spectral acceleration," *IEEE Trans. Antennas Propag.*, Vol. 55, No. 12, 3576–3586, Dec. 2007.
7. Zamani, H., A. Tavakoli, and M. Dehmollaian, "Scattering from layered rough surfaces: Analytical and numerical investigations," *IEEE Trans. Geosci. Rem. Sens.*, Vol. 54, No. 6, 3685–3696, Jun. 2016.
8. Yang, Y. and K.-S. Chen, "Full-polarization bistatic scattering from an inhomogeneous rough surface," *IEEE Trans. Geosci. Remote Sens.*, Vol. 57, No. 9, 6434–6446, Sep. 2019.
9. Jonard, F., F. Andé, N. Pinel, C. Warren, H. Vereecken, and S. Lambot, "Modeling of multilayered media Green's functions with rough interfaces," *IEEE Trans. Geosci. Remote Sens.*, Vol. 57, No. 10, 7671–7681, Oct. 2019.
10. Tijhuis, A. G., *Electromagnetic Inverse Profiling: Theory and Numerical Implementation*, VNU, Utrecht, The Netherlands, 1987.
11. Ghosh Roy, D. N. and L. S. Couchman, *Inverse Problems and Inverse Scattering of Plane Waves*, Academic Press, London, 1996.
12. Afifi, S. and M. Diaf, "Scattering by random rough surfaces: Study of direct and inverse problem," *Optics Comm.*, Vol. 265, 11–17, 2006.
13. Tabatabaeenejad, A. and M. Moghaddam, "Inversion of subsurface properties of layered dielectric structures with random slightly rough interfaces using the method of simulated annealing," *IEEE Trans. Geosci. Remote Sensing*, Vol. 47, No. 7, 2035–2046, Jul. 2009.
14. Elson, J. M., "Infrared light scattering from surfaces covered with multiple dielectric overlayers," *Appl. Opt.*, Vol. 16, No. 11, 2873–2881, Nov. 1977.
15. Elson, J. M., J. P. Rahn, and J. M. Bennett, "Relationship of the total integrated scattering from multilayer-coated optics to angle of incidence, polarization, correlation length, and roughness cross-correlation properties," *Appl. Opt.*, Vol. 22, No. 20, 3207–3219, Oct. 1983.
16. Fuks, I. M., "Wave diffraction by a rough boundary of an arbitrary plane-layered medium," *IEEE Trans. Antennas Propag.*, Vol. 49, No. 4, 630–639, Apr. 2001.
17. Tabatabaeenejad, A. and M. Moghaddam, "Bistatic scattering from three-dimensional layered rough surfaces," *IEEE Trans. Geosci. Remote Sens.*, Vol. 44, No. 8, 2102–2114, Aug. 2006.
18. Imperatore, P., A. Iodiceand, and D. Riccio, "Electromagnetic wave scattering from layered structures with an arbitrary number of rough interfaces," *IEEE Trans. Geosci. Remote Sens.*, Vol. 47, No. 4, 1056–1072, Apr. 2009.
19. Afifi, S., R. Duséaux, and R. de Oliveira, "Statistical distribution of the field scattered by rough layered interfaces: Formulae derived from the small perturbation method," *Waves Random Complex Media*, Vol. 20, No. 1, 1–22, Feb. 2010.

20. Afifi, S. and R. Dusséaux, "Scattering by anisotropic rough layered 2D interfaces," *IEEE Trans. Antenna Propagat.*, Vol. 60, No. 11, 5315–5328, Nov. 2012.
21. Zamani, H., A. Tavakoli, and M. Dehmollaian, "Scattering from two rough surfaces with inhomogeneous dielectric profiles," *IEEE Trans. Antenna. Propag.*, Vol. 63, No. 12, 5753–5766, Dec. 2015.
22. Van Laarhoven, P. J. M. and E. H. L. Aarts, *Simulated Annealing: Theory and Applications*, Reidel, Dordrecht, The Netherlands, 1987.
23. Kirkpatrick, S., C. D. Gelatt, and M. P. Vecchi, "Optimization by simulated annealing," *Science*, Vol. 220, No. 4598, 671–680, May 1983.
24. Kirkpatrick, S., "Optimization by simulated annealing: Quantitative studies," *J. Stat. Phys.*, Vol. 34, No. 5/6, 975–986, Mar. 1984.
25. Corana, A., M. Marchesi, C. Martini, and S. Ridella, "Minimizing multimodal functions of continuous variables with the "simulated annealin" algorithm," *ACM Trans. Math. Soft.*, Vol. 13, No. 3, 262–280, Sep. 1987.
26. Lee, K.-C., "Frequency-domain analyses of non-linearly loaded antenna arrays using simulated annealing algorithms," *Progress In Electromagnetics Research*, Vol. 53, 271–281, 2005.
27. Voronovich, G., *Wave Scattering from Rough Surfaces*, Springer, Berlin, 1994.
28. Voronovich, G., "Small-slope approximation for electromagnetic wave scattering at a rough interface of two dielectric half-spaces," *Wave Random Media*, Vol. 4, 337–367, 1994.
29. Berrouk, A., R. Duséaux, and S. Afifi, "Electromagnetic wave scattering from rough layered interfaces: Analysis with the small perturbation method and the small slope approximation," *Progress In Electromagnetics Research B*, Vol. 57, 177–190, 2014.
30. Afifi, S., R. Dusséaux, and A. Berrouk, "Electromagnetic scattering from 3D layered structures with randomly rough interfaces: Analysis with the small perturbation method and the small slope approximation," *IEEE Trans. Ant. Prop.*, Vol. 62, No. 10, 5200–5208, Oct. 2014.
31. Duséaux, R., S. Afifi, and M. Dechambre, "Scattering properties of a stratified air/snow/sea ice medium. Small slope approximation," *Comptes Rendus Physique*, Vol. 17, No. 9, 995–1002, Elsevier Masson, 2016.
32. Jackson, D. R. and D. R. Olson, "The small-slope approximation for layered, fluid seafloors," *J. Acoust. Soc. Am.*, Vol. 147, 56–73, 2020.
33. Beckmann, P. and A. Spizzichino, *The Scattering of Electromagnetic Waves from Rough Surfaces*, Pergamon Press, Oxford, UK, 1963.
34. Chen, Q., D. Won, and D. M. Akos, "Snow depth estimation accuracy using a dual-interface GPS-IR model with experimental results," *GPS Solut.*, Vol. 21, 211–223, 2017.
35. Lemmetyinen, J., M. Schwank, K. Rautiainen, A. Kontu, T. Parkkinen, C. Mätzler, A. Wiesmann, U. Wegüller, C. Derksen, P. Toose, A. Roy, and J. Pulliainen, "Snow density and ground permittivity retrieved from L-band radiometry: Application to experimental data," *Remote Sensing of Environment*, Vol. 180, 377–391, 2016.
36. Frolov, A. D. and Y. Y. Macheret, "On dielectric properties of dry and wet snow," *Hydrol. Process.*, Vol. 13, 1755–1760, 1999.
37. Kennedy, J. and R. Eberhart, "Particle swarm optimization," *Proc. IEEE of International Conference on Neural Networks*, 1942–1948, 1995.
38. Holland, J. H., *Adaptation in Natural and Artificial Systems*, University of Michigan Press, Ann Arbor, MI, 1975.
39. Tso, B. C. K. and P. M. Mather, "Classification of multisource remote sensing imagery using a genetic algorithm and Markov random fields," *IEEE Trans. Geosci. Remote Sens.*, Vol. 37, No. 3, 1255–1260, May 1999.